Journal Name

ARTICLE TYPE

Cite this: DOI: 00.0000/xxxxxxxxxx

Reversible and irreversible colossal barocaloric effects in plastic crystals

Araceli Aznar,[a] Pol Lloveras,*[a] María Barrio,[a] Philippe Negrier,[b] Antoni Planes,[c] Lluís Mañosa,[c] Neil D. Mathur,[d] Xavier Moya,[d] and Josep-Lluís Tamarit[a]

Received Date
Accepted Date

DOI: 00.0000/xxxxxxxxxx

The extremely large latent heats exchanged in phase transitions involving strong molecular orientational disordering have recently led to propose plastic crystals as a feasible solution for solid-state barocaloric eco-friendly cooling technologies. Here we determine the reversible barocaloric response of four plastic crystals derived from neopentane [$C(CH_3)_4$]: $(NH_2)C(CH_2OH)_3$ (TRIS for short), $(NH_2)(CH_3)C(CH_2OH)_2$ (AMP), $(CH_3)C(CH_2OH)_3$ (PG) and $(CH_3)_3C(CH_2OH)$ (NPA). All of them display colossal entropy changes at their ordered-plastic phase transition, which is a primal requirement for competitive barocaloric materials. However, we show that it is also important to verify that the large barocaloric effects can be achieved using pressures that, while being moderate, are large enough to overcome the pressure-dependent hysteresis. From this quantity and using the quasi-direct method, we determine the minimum pressure needed to achieve reversible barocaloric effects, p_{rev}, for each compound. Specifically, we find a small and moderate p_{rev} for PG and NPA, respectively, which therefore display colossal reversible barocaloric effects comparable to harmful fluids used in current refrigerators and thus confirm the potential of plastic crystals as excellent alternatives. Instead, in TRIS and AMP, the obtained p_{rev} is excessive to yield reversible barocaloric effects useful for cyclic applications.

1 Introduction

Caloric effects across solid-state first-order phase transitions offer the possibility of controlling the exchange of latent heat by means of an external field. In view of the climate change emergency, caloric effects are being investigated for cooling applications as an alternative to replace current compressors that use greenhouse gases[1]. Most likely, finding appropriate solid materials has become the major hindrance for a commercial implementation. In addition to problems such as cost and toxicity, other more fundamental problems are encountered when looking for good caloric materials. Generally, this rational search is based on the knowledge of few requirements that are often accessible using widely extended conventional experimental techniques and/or available in the literature, that are a phase transition with large latent heat close to a desired operational temperature and a high sensitivity of the phase transition with the applied field[2,3].

Despite caloric prototypes are showing high efficiencies[1,4], the relatively small latent heats in most solid-solid transitions cannot compete against those exchanged in liquid-vapor transitions used in current compressors, which results in a refrigeration capacity significantly smaller. However, this paradigm could change due to the recent identification[5,6] of a family of materials named plastic crystals. Some compounds in this family undergo first-order phase transitions with enormous latent heat mainly due to an unusual strong molecular orientational disordering, for which they have traditionally attracted interest for passive thermal energy storage applications[7,8]. On the other hand, their strongly non-isochoric transitional character makes the associated huge enthalpy changes be easily driven by pressure and therefore they have now been proposed for barocaloric (BC) effects. Following this advance, a list with a number of plastic crystals with similar nominal characteristics has been suggested as potential excellent BC candidates[6]. However, while the criteria of large latent heat and sensitivity with the applied field are a necessary filter to discard useless materials, they are not sufficient to determine appropriate compounds. Other not less important conditions must be fulfilled by the candidates in order to exhibit a good caloric performance as, for instance, good reversibility and maintenance of proper thermodynamic transition properties (i.e. large transition entropy and volume changes and sharp transition) at high applied

[a] Grup de Caracterització de Materials, Departament de Física, EEBE and Barcelona Research Center in Multiscale Science and Engineering, Universitat Politècnica de Catalunya, Eduard Maristany, 10-14, 08019 Barcelona, Catalonia.* E-mail: pol.lloveras@upc.edu
[b] Université de Bordeaux, LOMA, UMR 5798, F-33400 Talence, France
[c] Departament de Física de la Matèria Condensada, Facultat de Física, Universitat de Barcelona, Martí i Franquès 1, 08028 Barcelona, Catalonia
[d] Department of Materials Science, University of Cambridge, Cambridge, CB3 0FS, UK

fields.

Since cooling devices operate cyclically, the caloric effects used therein must be driven reversibly upon an indefinite sequence of application and removal of the external field, and therefore they may be dramatically affected by hysteresis. Near first-order phase transitions, the transition hysteresis introduces a history dependence in the system response to external stimuli such that caloric effects associated with the transition are irreversible below a certain threshold for the external field. Consequently, the necessary input work is increased and the temperature range of operation decreases so that the actual material performance decreases with respect to the ideal non-hysteretic frame. Although the key role of hysteresis for reversibility was well established almost one decade ago[9–11], a significant number of studies on caloric effects do not address this issue yet. Promising materials have been declared without revealing the hysteresis width[6,12–14] or reporting hysteresis widths that would entail manifestly excessive fields for a practical implementation[13,15–17]. While these considerations do not invalidate previous works, it is undoubtedly important to have information about such features whenever possible for the purpose of practical applications.

The aim of the present study is to check these important features in four plastic crystals that were enumerated in the aforementioned published list of excellent BC candidates[6], where reversibility and high-pressure properties were not taken into account. We show that, despite all of them exhibit nominal outstanding transition characteristics, two of them do not meet the expectations and do not demonstrate aptitude for BC applications. Our selected compounds belong to the family of neopentane [$C(CH_3)_4$] derivatives for which the methyl groups have been substituted by amino (NH_2) or hydroxymethyl (CH_2OH) groups: $(NH_2)C(CH_2OH)_3$ [2-amino-2-(hydroxymethyl)propane-1,3-diol, TRIS], $(NH_2)(CH_3)C(CH_2OH)_2$ [2-amino-2-methyl-1,3-propanediol, AMP], $(CH_3)C(CH_2OH)_3$ [2-hydroxymethyl-2-methyl-1,3-propanediol, PG] and $(CH_3)_3C(CH_2OH)$, [2,2-dimethyl-1-propanol, NPA]. Below the melting, at high temperature these molecules arrange in a cubic lattice: bcc ($Im\bar{3}m$) for those containing amino groups, otherwise fcc ($Fm\bar{3}m$), hereafter referred to as phase I, and exhibit dynamically disordered molecular orientations. On cooling across a first-order phase transition, they order completely accompanied by a symmetry reduction and a significant finite volume decrease. In particular, AMP, TRIS, NPA and PG adopt monoclinic[18] (space group undetermined), orthorhombic ($Pna2_1$)[19], triclinic[20] (space group undetermined) and tetragonal (bct, $I\bar{4}$)[18] structures respectively, hereafter referred to as phase II. This chemical and structural information is summarized in table 1.

All these transitions show entropy changes of hundreds of J K^{-1} kg^{-1} and large volume changes, which clearly point them as candidates for BC applications. However, our analysis reveals that both TRIS and AMP are unfeasible due to an insourmountable hysteresis at reasonable pressures, whereas instead PG and NPA demonstrate an excellent BC performance.

2 Experimental

Powdered samples of TRIS ($\geq$99.8% purity), PG (99%) and NPA (99%) were purchased from Sigma-Aldrich and AMP ($\geq$99.5%) was purchased from Fluka and used as received. Calorimetry at normal pressure was carried out using a conventional Differential Scanning Calorimeter Q100 from TA Instruments. Pressure-dependent calorimetry was performed on two different high-pressure differential thermal analyzers. One high-pressure cell is a custom-built irimo block that uses Bridgman thermal sensors and operates up to 3 kbar within a temperature range from room-temperature to 473 K controlled by a resistive heater. The other one is a high-pressure Cu-Be cell from Unipress (Poland) that uses Peltier Modules as thermal sensors and operates up to 6 kbar within a temperature range from 200 K to 393 K controlled by an external thermal bath. In both cells, few hundreds of mg of each sample were mixed with a perfluorinated inert fluid (Galden Bioblock Scientist) to remove air and encapsulated in tin capsules. The pressure-transmitting fluid was DW-Therm M90.200.02 (Huber). Calorimetry measurements coherently yielded positive $dQ/|dT| \equiv \dot{Q}/|\dot{T}|$ peaks corresponding to the endothermic (II→I) transitions and negative $dQ/|dT|$ peaks corresponding to the exothermic (I→II) transitions. The respective transition temperatures, $T_{\mathrm{II}\to\mathrm{I}}$ and $T_{\mathrm{I}\to\mathrm{II}}$, were determined from the onset of the calorimetric peaks. Transition enthalpy changes $\Delta H_{\mathrm{II}\to\mathrm{I}}$ and $\Delta H_{\mathrm{I}\to\mathrm{II}}$, and transition entropy changes $\Delta S_{\mathrm{II}\to\mathrm{I}}$ and $\Delta S_{\mathrm{I}\to\mathrm{II}}$, were determined from integrations of $dQ/d|T|$ and of $(1/T)dQ/d|T|$ peaks after baseline subtraction, respectively.

3 General aspects on reversibility and hysteresis

For a reliable estimation of reversible caloric effects, direct and quasi-direct methods are normally preferable over indirect measurements[2] as the use of the thermodynamic Maxwell relation may fail due to misleading protocols[21,22] or strong out-of-equilibrium dynamics[23–25]. While direct methods naturally yield reversible effects because they involve the same changing-field dynamics, quasi-direct methods are carried out by changing temperature at constant applied fields[2] so that in these cases the determination of reversible effects needs transferring the measured isofield thermally-driven hysteretic effects to isothermal field-driven hysteretic effects via calculations. In this respect, comparison between direct and quasi-direct experimental data has shown that reversible isothermal entropy changes ΔS_{rev} can be obtained from the overlapping between isothermal entropy changes ΔS derived from isofield measurements performed on heating and on cooling independently[11,26] (see Fig. 1a,c). For materials displaying conventional BC effects ($dT_{\mathrm{II}\leftrightarrow\mathrm{I}}/dp(p) > 0$, where II↔I means the set of II→I and I→II), and assuming hereafter that BC effects will take place always with the lower pressure being atmospheric pressure, p_{atm}, the overlapping condition entails that the minimum pressure, p_{rev}, to achieve nonzero ΔS_{rev} is given by the value at which the exothermic transition temperature equals the endothermic transition temperature at atmospheric pressure, i.e.,

Table 1 Chemical and structural details for the plastic crystals under study.

Abbreviation	Chemical formula	Amino group	Structure of phase I	Structure of phase II
TRIS	$(NH_2)C(CH_2OH)_3$	yes	bcc ($Im\bar{3}m$)	orthorhombic ($Pna2_1$)
PG	$(CH_3)C(CH_2OH)_3$	no	fcc ($Fm\bar{3}m$)	tetragonal (bct, $I\bar{4}$)
AMP	$(NH_2)(CH_3)C(CH_2OH)_2$	yes	bcc ($Im\bar{3}m$)	monoclinic
NPA	$(CH_3)_3C(CH_2OH)$	no	fcc ($Fm\bar{3}m$)	triclinic

$T_{\mathrm{I}\to\mathrm{II}}(p_{\mathrm{rev}}) = T_{\mathrm{II}\to\mathrm{I}}(p_{\mathrm{atm}})$. From this equality, we can write

$$p_{\mathrm{rev}} = \int_{T_{\mathrm{I}\to\mathrm{II}}(p_{\mathrm{atm}})}^{T_{\mathrm{II}\to\mathrm{I}}(p_{\mathrm{atm}})} \left(\frac{dT_{\mathrm{I}\to\mathrm{II}}}{dp}\right)^{-1} dT. \quad (1)$$

If $\left(\frac{dT_{\mathrm{I}\to\mathrm{II}}}{dp}\right)$ is constant, then $p_{\mathrm{rev}} = \left(\frac{dT_{\mathrm{I}\to\mathrm{II}}}{dp}\right)^{-1} \Delta T_{\mathrm{II}\leftrightarrow\mathrm{I}}(p_{\mathrm{atm}})$ where $\Delta T_{\mathrm{II}\leftrightarrow\mathrm{I}}(p_{\mathrm{atm}})$ is the thermal hysteresis at atmospheric pressure defined as $\Delta T_{\mathrm{II}\leftrightarrow\mathrm{I}}(p_{\mathrm{atm}}) = T_{\mathrm{II}\to\mathrm{I}}(p_{\mathrm{atm}}) - T_{\mathrm{I}\to\mathrm{II}}(p_{\mathrm{atm}})$. Instead, the minimum pressure to obtain reversible adiabatic temperature changes ΔT_{rev} is usually higher than p_{rev}. In particular,

$$p_{\mathrm{rev}}^{\Delta T} = \int_{T_{\mathrm{I}\to\mathrm{II}}^{f}(p_{\mathrm{atm}})}^{T_{\mathrm{II}\to\mathrm{I}}(p_{\mathrm{atm}})} \left(\frac{dT_{\mathrm{I}\to\mathrm{II}}}{dp}\right)^{-1} dT. \quad (2)$$

where we denote as $T_{\mathrm{I}\to\mathrm{II}}^{f}(p_{\mathrm{atm}})$ the finishing temperature on cooling across the transition I→II (see Fig. 1b,d). Notice that for ideal perfectly isothermal transitions, the ranges for ΔT_{rev} and ΔS_{rev} are the same because $T_{\mathrm{I}\to\mathrm{II}}^{f} = T_{\mathrm{I}\to\mathrm{II}}$.

Therefore, $\Delta T_{\mathrm{II}\leftrightarrow\mathrm{I}}(p)$ and $dT_{\mathrm{I}\to\mathrm{II}}/dp(p)$ represent key properties in the study of the viability of BC materials, which can be generalized to any other caloric effect. Moreover, if cycles involving lowest pressures above normal pressure are considered, then the knowledge of $dT_{\mathrm{II}\to\mathrm{I}}/dp(p)$ is also required. It is worth pointing out here that for materials exhibiting inverse behavior ($dT_{\mathrm{I}\leftrightarrow\mathrm{II}}/dp(p) < 0$) the same quantities need to be evaluated for the inverse transitions.

In addition, establishing the dependence of the transition thermodynamic quantities on the applied pressure[27] has been shown to become important because a possible but a priori unknown decrease of the transition entropy change with pressure might reduce substantially the caloric performance. This has been observed to occur, for instance, in some magnetostructural[28,29], ferroelectric[30,31] and hybrid organic-inorganic systems[32]. Otherwise, omitting this feature may lead to large uncertainties or inexact conclusions such as a systematic overestimation of the caloric effects or false expectations.

4 Results and discussion

Calorimetry measurements performed at atmospheric pressure carried out for all compounds (not shown) yield endothermic (II→I) and exothermic (I→II) transition properties listed in Table 2. The endothermic values are in overall agreement with reported literature data[19,33] and confirm their colossal transition entropy changes. The exothermic values have not been reported so far and the differences from endothermic values arise due to the transition hysteresis.

4.1 Contributions to the transition entropy change

In the compounds under study, the total entropy change can be divided into two contributions: $\Delta S_{\mathrm{II}\to\mathrm{I}} = \Delta S_{\mathrm{II}\to\mathrm{I}}^{e} + \Delta S_{\mathrm{II}\to\mathrm{I}}^{c}$ where the first term arises from the lattice distortion whereas the second term originates in the release of different orientational conformations.

The strain entropy change can be calculated with respect to the unstrained cubic phase in therms of the Helmholtz free energy F^e as $\Delta S_{\mathrm{II}\to\mathrm{I}}^{e} = S^e(\mathrm{I}) - S^e(\mathrm{II}) = -S^e(\mathrm{II}) = \left(\frac{\partial F_{\mathrm{II}}^{e}}{\partial T}\right)_e$, where e refers to the strain. In the cubic system, F^e can be written up to the harmonic approximation as $F^e = Ke_1^2 + C'(e_2^2+e_3^2) + C_{44}(e_4^2+e_5^2+e_6^2)$. Here, $K = \frac{C_{11}+2C_{21}}{3}$ and $C' = \frac{C_{11}-C_{12}}{2}$ are the bulk and deviatoric moduli respectively, with C_{ij} being components of the stiffness tensor, and e_i are the symmetry-adapted strains[34] of the cubic system corresponding to volumic (e_1), deviatoric (e_2 and e_3) and shear strains (e_4, e_5 and e_6). On the other hand, the experimental measurement of elastic constants in plastic crystals is hard due to the difficulty in growing large single crystals, and available literature data are absent for the compounds under study. To estimate the order of magnitude, we have used elastic constants as a function of temperature for plastic crystal fullerene C_{60} which, averaged over the full reported[35] temperature range in the ordered phase, yield $\frac{\partial K}{\partial T} \sim -3.8\cdot10^7$ GPa K^{-1}, $\frac{\partial C'}{\partial T} \sim -4.7\cdot10^6$ GPa K^{-1} and $\frac{\partial C_{44}}{\partial T} \sim -2.0\cdot10^7$ GPa K^{-1}. For PG, the lattice parameters near the fcc-bct deformation[20] are $a_{\mathrm{I}} = 8.876$ Å, $a_{\mathrm{II}} = 6.052$ Å and $c_{\mathrm{II}} = 8.872$ Å, which correspond to[36] the symmetry-adapted strains $e_1 = -0.046$, $e_3 = 0.032$ and $e_2 = e_4 = e_5 = e_6 = 0$. Therefore, taking a density of $\rho = 1.23$ g cm^{-3}, we obtain an entropy change associated with the deviatoric strain $\Delta S_{\mathrm{II}\to\mathrm{I}}^{d} \simeq 4$ J K^{-1} kg^{-1} and an entropy change associated with the volume change $\Delta S_{\mathrm{II}\to\mathrm{I}}^{V} \simeq 67$ J K^{-1} kg^{-1}, which are significantly smaller than the total entropy change, $\Delta S_{\mathrm{II}\to\mathrm{I}} \simeq 485$ J K^{-1} kg^{-1}. For the remaining compounds, the reconstructive nature of the analyzed phase transitions in those cases prevents establishing a correspondence between the unstrained and the strained lattices and therefore the strain entropy change has no meaning.

Alternatively, the volumic entropy change can be approximately estimated as $\Delta S_{\mathrm{II}\to\mathrm{I}}^{V} = (\langle\alpha\rangle / \langle\beta\rangle)\Delta V_{\mathrm{II}\to\mathrm{I}}$, where $\langle\alpha\rangle$ and $\langle\beta\rangle$ correspond to the thermal expansion and the isothermal compressibility, respectively, averaged over the two phases close to the phase transition[37,38]. Using dilatometry and x-ray diffraction data for NPA from Refs[39,40] we find $\Delta S_{\mathrm{II}\to\mathrm{I}}^{V} \sim 52 \pm 10$ J K^{-1} kg^{-1}, which is considerably smaller than the total entropy change, $\Delta S_{\mathrm{II}\to\mathrm{I}} \sim 200$ J K^{-1} kg^{-1}. Although a complete set of data is not available in the literature for any of the remaining compounds, existing data[19,41,42] strongly indicate that for PG $\Delta S_{\mathrm{II}\to\mathrm{I}}^{V} \sim 80 \pm 40$ J K^{-1} kg^{-1} (which is consistent with the calculation carried out above), for TRIS $\Delta S_{\mathrm{II}\to\mathrm{I}}^{V} \sim 90 \pm 50$ J K^{-1} kg^{-1}

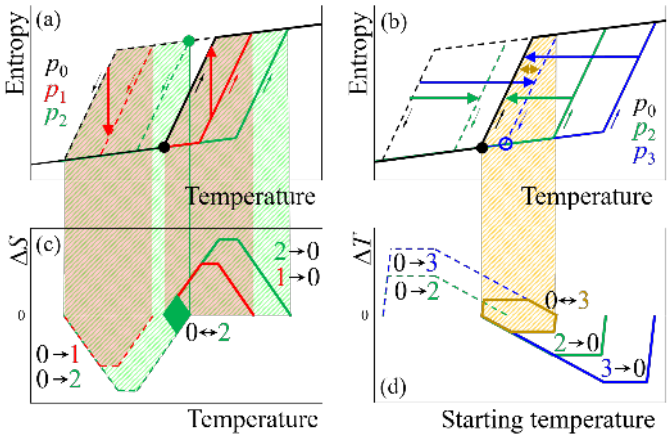

Fig. 1 Schematic representations of isobaric entropy-temperature curves and conventional BC effects to evaluate reversibility. (a,b) Isobaric entropies at different values of pressure p_0 (black), $p_1 > p_0$ (red), $p_2 > p_1$ (green) and $p_3 > p_2$ (blue) on heating (continuous lines) and on cooling (dashed lines) as indicated by the small arrows. In both panels, black filled circles denote the onset of the endothermic transition at pressure p_0 [$T_{\mathrm{II}\to\mathrm{I}}(p_0)$]. In panel (a) the green filled circle denotes the onset of the exothermic transition at p_2, $T_{\mathrm{I}\to\mathrm{II}}(p_2)$. In panel (b) the blue empty circle denotes the finishing temperature of the transition on cooling at pressure p_3, $T^f_{\mathrm{II}\to\mathrm{I}}(p_3)$. In panel (a), the red vertical downward (upward) arrow indicates the thermodynamic path used to calculate irreversible isothermal entropy changes ΔS on compression (decompression). In panel (b), the horizontal rightward (leftward) arrows indicate the thermodynamic paths used to calculate irreversible adiabatic temperature changes ΔT on compression (decompression). The left-right yellow arrow indicates the thermodynamic path used to calculate reversible ΔT. (c) Irreversible ΔS obtained under a pressure increase of $p_1 - p_0$ (red, dashed), under an increase of $p_2 - p_0$ (green, dashed), under a decrease of $p_0 - p_1$ (red, continuous) and under a decrease of $p_0 - p_2$ (green, continuous). The green colored area indicates the reversible ΔS obtained from overlapping the curves obtained on increasing and decreasing the field. (d) Irreversible ΔT obtained under a pressure increase of $p_2 - p_0$ (green, dashed), under an increase of $p_3 - p_0$ (blue, dashed), under a decrease of $p_0 - p_2$ (green, continuous) and under a decrease of $p_0 - p_3$ (blue, continuous). The dark yellow line indicates the reversible ΔT. Notice that ΔT are plotted as a function of the *starting* temperature because the system temperature changes along the adiabatic path.

and for AMP $\Delta S^V_{\mathrm{II}\to\mathrm{I}} \sim 100 \pm 50$ J K^{-1} kg^{-1}. These numbers for $\Delta S^V_{\mathrm{II}\to\mathrm{I}}$, even with such a prudent interval of uncertainty, lie in all cases well below half the corresponding total transition entropy changes $\Delta S_{\mathrm{II}\to\mathrm{I}}$, which means that for all compounds the major contribution to $\Delta S_{\mathrm{II}\to\mathrm{I}}$ emerges from the orientational disordering at the II→I transition, $\Delta S^c_{\mathrm{II}\to\mathrm{I}}$.

The contribution of the orientational disordering to these total entropy changes can be calculated as $\Delta S^c_{\mathrm{II}\to\mathrm{I}} = (RM^{-1})ln(N_{\mathrm{I}}/N_{\mathrm{II}})$, where R is the universal gas constant, M is the molar mass and N_{I} and N_{II} are the number of possible molecular conformations in phases I and II, respectively. While in general in plastic crystals phase II can still exhibit some disorder (i.e. $N_{\mathrm{II}} > 1$)[43–47], for all the compounds here studied $N_{\mathrm{II}} = 1$ can be reasonably assumed because hydrogen bonds do not permit any molecular disorder[48]. Notice, however, that in other cases the presence of hydrogen bonds may not be a sufficient condition either to have $N_{\mathrm{II}} = 1$[49]. With respect to the disordered phase, for those compounds with an fcc unit cell (PG and NPA, point group T_d, subgroup C_{3v}) there are 10 possible orientations whereas those with a bcc unit cell (AMP and TRIS, point group D_{2d}) there are 6 possible orientations[50]. For each orientation, PG, NPA, AMP and TRIS have 11, 3, 9 and 11 different conformations, respectively. Therefore, we obtain the following nominal values: For NPA, $\Delta S^c_{\mathrm{II}\to\mathrm{I}} = 321$ J K^{-1} kg^{-1}; for PG, $\Delta S^c_{\mathrm{II}\to\mathrm{I}} = 325$ J K^{-1} kg^{-1}; for TRIS, $\Delta S^c_{\mathrm{II}\to\mathrm{I}} = 287$ J K^{-1} kg^{-1}; for AMP $\Delta S^c_{\mathrm{II}\to\mathrm{I}} = 315$ J K^{-1} kg^{-1}. As expected, these values are substantially larger than the values obtained for the corresponding $\Delta S^V_{\mathrm{II}\to\mathrm{I}}$ but they are inconsistent with the values obtained for the total entropy change $\Delta S_{\mathrm{II}\to\mathrm{I}}$. This means that the information for $\Delta S^c_{\mathrm{II}\to\mathrm{I}}$ is incomplete. For instance, for NPA not all theoretically possible conformations are observed via Raman spectroscopy[51], which explains the overestimation of the aforegiven value for $\Delta S^c_{\mathrm{II}\to\mathrm{I}}$. In turn, for TRIS and AMP, additional $\pi/2$ rotations of the amino groups could take place, increasing the resulting $\Delta S^c_{\mathrm{II}\to\mathrm{I}}$. It is thus clear that an accurate determination for $\Delta S^c_{\mathrm{II}\to\mathrm{I}}$ requires further investigation and lies beyond the scope of this work.

4.2 Evaluation of barocaloric reversible ranges

To evaluate the minimum pressure p_{rev} above which ΔS_{rev} becomes nonzero, the use of eq. 1 requires the knowledge of $dT_{\mathrm{I}\to\mathrm{II}}/dp(p)$ and $\Delta T_{\mathrm{II}\leftrightarrow\mathrm{I}}(p_{\mathrm{atm}})$. In the following we analyze these two quantities and estimate p_{rev} for the compounds under study.

Values for $\Delta T_{\mathrm{II}\leftrightarrow\mathrm{I}}(p_{\mathrm{atm}})$ can be directly obtained from Table 2. With respect to $dT_{\mathrm{I}\to\mathrm{II}}/dp(p)$, its determination via the Clausius-Clapeyron (CC) equation, $\frac{dT_{\mathrm{II}\leftrightarrow\mathrm{I}}}{dp}(p) = \frac{\Delta V_{\mathrm{II}\to\mathrm{I}}}{\Delta S_{\mathrm{II}\to\mathrm{I}}}$, may be not reliable because (i) it is based on equilibrium conditions (i.e. endothermic, II→I transition) and (ii) $\Delta S_{\mathrm{II}\to\mathrm{I}}$ and $\Delta V_{\mathrm{II}\to\mathrm{I}}$ are usually available only at normal pressure. Consequently, significant differences between $dT_{\mathrm{II}\to\mathrm{I}}/dp$ at normal pressure, $dT_{\mathrm{II}\to\mathrm{I}}/dp(p_{\mathrm{atm}})$, (as derived from CC) and $dT_{\mathrm{I}\to\mathrm{II}}/dp(p)$ at high pressure can arise. In summary, atmospheric-pressure data can be used as a rough estimate only as they may lead to large uncertainties or incorrect conclusions. Therefore, to rigorously determine the actual reversible ranges of pressure via the quasi-direct method, the knowledge of the exothermic transition temperatures as a function of pressure, $T_{\mathrm{I}\to\mathrm{II}}(p)$, is imperative. To derive these values we perform pressure-dependent isobaric calorimetry on heating and cooling across the II↔I transition at temperature rates $|\dot{T}| \sim 2-4$ K min^{-1} (see Fig. 2a-d). The pressure-dependent transition temperatures determined from the peak onsets (see Fig. 2e-h) confirm the aforementioned discrepancies between $dT_{\mathrm{II}\to\mathrm{I}}/dp$ at p_{atm} and at $p > p_{\mathrm{atm}}$ and $dT_{\mathrm{I}\to\mathrm{II}}/dp$ for all pressures. For TRIS (see Fig. 2e) the hysteresis $\Delta T_{\mathrm{II}\leftrightarrow\mathrm{I}}(p)$ increases with increasing pressure because for all pressures we obtain $dT_{\mathrm{II}\to\mathrm{I}}/dp = 3.7 \pm 0.2$ K kbar^{-1} $> dT_{\mathrm{I}\to\mathrm{II}}/dp = 1.5 \pm 0.6$ K kbar^{-1}. The latter magnitude is clearly insufficient to overcome $\Delta T_{\mathrm{II}\leftrightarrow\mathrm{I}}(p_{\mathrm{atm}}) \sim 75$ K at reasonable pressures, as eq. 1 renders $p_{\mathrm{rev}} \sim 50$ kbar. For PG (see Fig. 2f) the hysteresis $\Delta T_{\mathrm{II}\leftrightarrow\mathrm{I}}(p_{\mathrm{atm}}) \sim 3.7$ K can be easily overcome given the magnitude for $dT_{\mathrm{I}\to\mathrm{II}}/dp = 9.4 \pm 0.3$ K kbar^{-1}, which yields a low reversible threshold $p_{\mathrm{rev}} \sim 0.4$ kbar. In this case, $\Delta T_{\mathrm{II}\leftrightarrow\mathrm{I}}(p)$ decreases with increasing pressure because for all pressures $dT_{\mathrm{I}\to\mathrm{II}}/dp = 9.4 \pm 0.3$ K kbar^{-1} $> dT_{\mathrm{II}\to\mathrm{I}}/dp = 7.9 \pm 0.3$

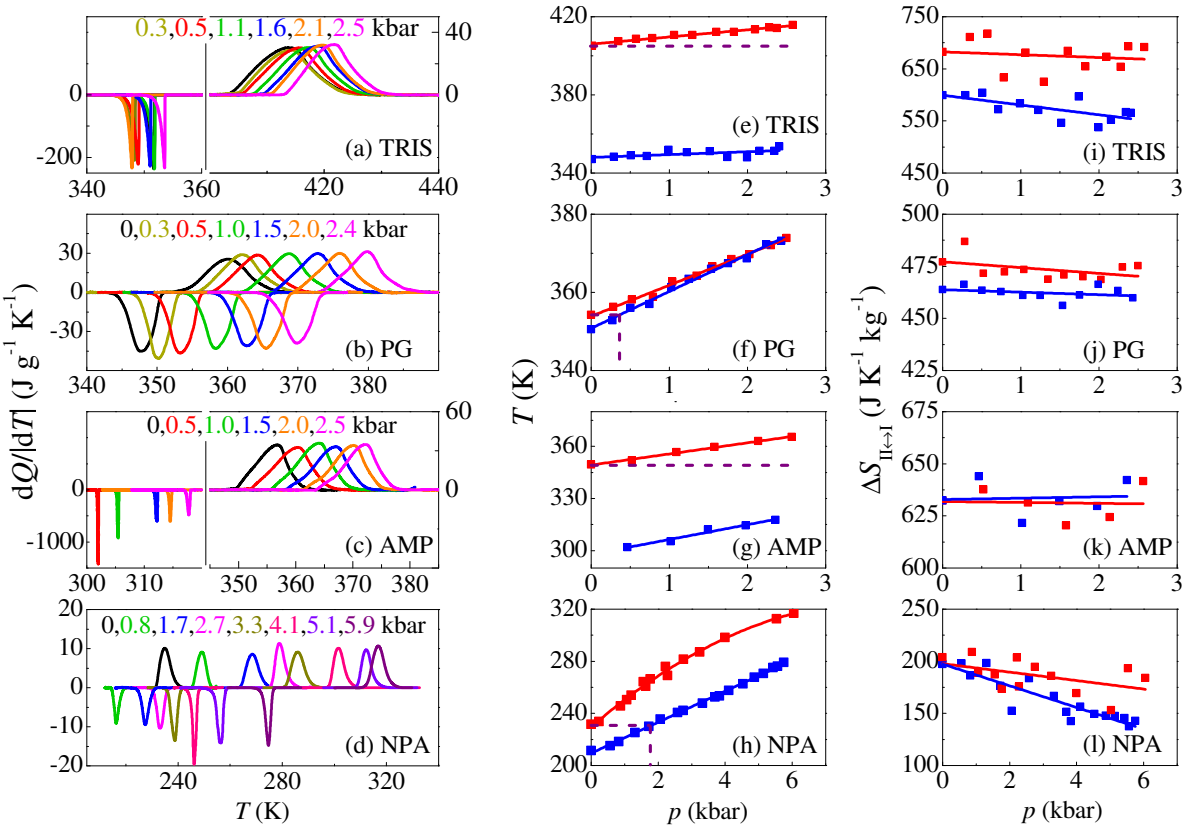

Fig. 2 (a-d): Isobaric calorimetry at selected pressures on heating (positive) and cooling (negative) for (a) TRIS, (b) PG, (c) AMP and (d) NPA. (e-h): Temperature-pressure phase diagram on heating (red data) and on cooling (blue data) for (e) TRIS, (f) PG, (g) AMP and (h) NPA. (i-l): Pressure-dependent transition entropy changes on heating ($T_{\mathrm{II}\to\mathrm{I}}(p)$, red data) and on cooling ($T_{\mathrm{I}\to\mathrm{II}}(p)$, blue data) for (i) TRIS, (j) PG, (k) AMP and (l) NPA. Lines are fits to the data. Dashed horizontal purple line indicates the endothermic transition temperature and dashed vertical line indicates the pressure at which the exothermic transition temperature is equal to the endothermic transition temperature at normal pressure, which is the minimum pressure, p_{rev}, required to obtain reversible barocaloric effects.

K kbar^{-1}. Notice that the improper use of the latter value in eq. 1 would give rise to the overestimated value $p_{\mathrm{rev}} \sim 0.5$ kbar. As for AMP (see Fig. 2g), exothermic transitions are obtained with large hysteresis close to normal pressures ($\Delta T_{\mathrm{II}\leftrightarrow\mathrm{I}}(p \sim 0.5$ kbar$) \sim 50$ K), slightly decreasing with increasing pressure because for all pressures $dT_{\mathrm{II}\to\mathrm{I}}/dp = 6.4 \pm 0.2$ K kbar^{-1} $< dT_{\mathrm{I}\to\mathrm{II}}/dp = 8.5 \pm 0.7$ K kbar^{-1}, but still too large to be overcome by moderate pressures given the relatively small $dT_{\mathrm{I}\leftrightarrow\mathrm{II}}/dp$. In particular we obtain $p_{\mathrm{rev}} \sim 6$ kbar. Concerning NPA, it exhibits $dT_{\mathrm{II}\to\mathrm{I}}/dp(p_{\mathrm{atm}}) = 22 \pm 1$ K kbar^{-1} but $dT_{\mathrm{II}\to\mathrm{I}}/dp(p \sim 6$ kbar$) = 7 \pm 2$ K kbar^{-1} and, more importantly, $dT_{\mathrm{I}\to\mathrm{II}}/dp = 11.9 \pm 0.2$ K kbar^{-1} for all pressures. Given these values (and using $\Delta T_{\mathrm{II}\leftrightarrow\mathrm{I}}(p_{\mathrm{atm}}) \sim 23$ K), we obtain $p_{\mathrm{rev}} \sim 1.9$ kbar which in this case is twice larger than that expected from endothermic data or CC equation at atmospheric pressure. In fact, the out-of-equilibrium $T-p$ diagrams shown in Figs 2e-h permit to establish graphically the reversible threshold p_{rev} as indicated by the dashed purple lines according to the aforementioned condition $T_{\mathrm{I}\to\mathrm{II}}(p_{\mathrm{rev}}) = T_{\mathrm{II}\to\mathrm{I}}(p_{\mathrm{atm}})$. A summary of the transition characteristics at atmospheric pressure and values for p_{rev} is given in Table 2.

4.3 Construction of isobaric entropy curves

To calculate the BC effects using the quasi-direct method, we have computed the isobaric entropy curves $S'(T,p)$ at different pressures with respect to a reference value taken at normal pressure and at a temperature T_0 arbitrarily chosen well below the I→II transition temperature for each compound (see Fig. 3) so that $S'(T,p) = S(T,p) - S(T_0, p_{\mathrm{atm}})$. For this purpose we have followed the procedure described in Refs[5,52,53] according to which we need integration of our pressure-dependent calorimetric peaks after baseline subtraction and temperature-dependent heat capacity C_p from literature (NPA:[54]; AMP:[55]; PG:[56]; TRIS:[57,58]). The fact that C_p data is available only at normal pressure prevents us to determine the pressure dependence of the isobaric entropy in each phase directly from this quantity. However, this lack can be compensated by the use of the Maxwell relation $\Delta S_+(p_{\mathrm{atm}} \to p_1) = -\int_{p_{\mathrm{atm}}}^{p_1} (\partial V/\partial T)_p dp$, which establishes the entropy change when a pressure is applied in isothermal conditions outside the transition. In particular, given the conventional character of our materials, we include ΔS_+ in phase II[30]. To calculate ΔS_+, $(\partial V/\partial T)_p$ is taken from literature (NPA:[39], AMP:[59]; TRIS:[42]; PG:[60]) and assumed to be independent of pressure within the range under study, which is a reasonable assumption as derived from Refs[5,40,41]. Nonetheless, it can be estimated that

Table 2 Thermodynamic properties for both endothermic (II→I) and exothermic (I→II) transitions measured at atmospheric pressure.

Compd	$T_{\mathrm{II}\to\mathrm{I}}$	$T_{\mathrm{I}\to\mathrm{II}}$	$\frac{dT_{\mathrm{II}\to\mathrm{I}}}{dp}$	$\frac{dT_{\mathrm{I}\to\mathrm{II}}}{dp}$	$\Delta H_{\mathrm{II}\to\mathrm{I}}$	$\Delta H_{\mathrm{I}\to\mathrm{II}}$	$\Delta S_{\mathrm{II}\to\mathrm{I}}$	$\Delta S_{\mathrm{I}\to\mathrm{II}}$	p_{rev}
	K	K	K kbar^{-1}	K kbar^{-1}	J g^{-1}	J g^{-1}	J K^{-1} kg^{-1}	J K^{-1} kg^{-1}	kbar
TRIS	406.8 ± 0.5	331.2 ± 0.5	3.7 ± 0.2	1.5 ± 0.6	280 ± 5	203 ± 5	682 ± 13	599 ± 12	∼50
PG	354.2 ± 0.5	350.5 ± 0.5	7.9 ± 0.2	9.4 ± 0.3	176 ± 4	164 ± 4	485 ± 10	479 ± 10	∼0.4
AMP	352.7 ± 0.5	-	6.4 ± 0.4	8.5 ± 0.7	224 ± 5	-	632 ± 13	-	∼6
NPA	231.6 ± 0.5	211.3 ± 0.5	22 ± 1	11.9 ± 0.2	48.2 ± 2.0	40.4 ± 2.0	204 ± 5	197 ± 5	∼1.8

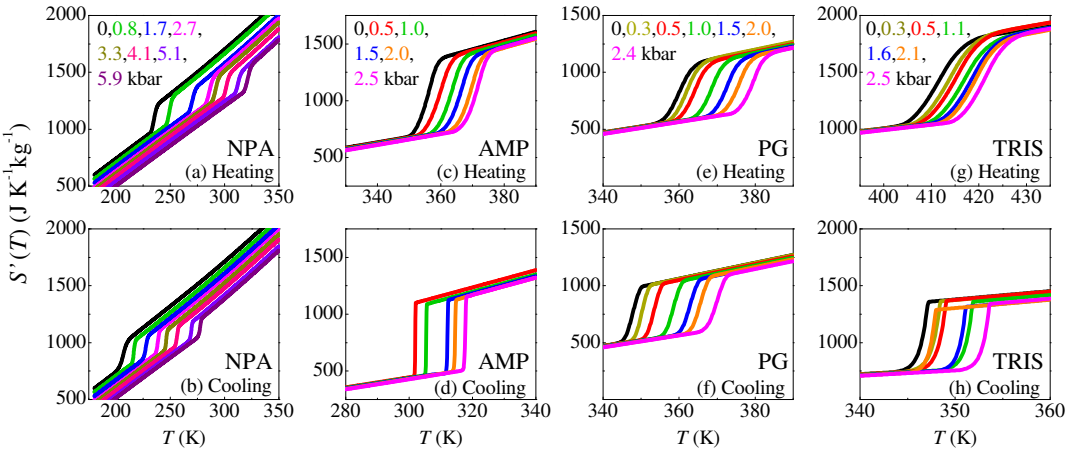

Fig. 3 Isobaric entropy curves at selected pressures with respect to a reference value taken at atmospheric pressure, on heating (top panels) and cooling (bottom panels) for (a,b) NPA, (c, d) AMP, (e,f) PG and (g,h) TRIS. Color legend for pressure values in top panels are also valid in the corresponding bottom panels. The isothermal distance between isobaric entropy curves in panels (a,b) originates from the relatively significant contribution of ΔS_+ in each side of the transition for NPA.

an uncertainty of 20% in $(\partial V/\partial T)_p$ would yield an error of $\sim 3\%$ in the BC effects obtained across the transition, which is smaller than the uncertainty interval of our results.

Although in some materials such as metallic alloys neglecting ΔS_+ may be irrelevant because $(\partial V/\partial T)_{p_{\mathrm{atm}}}$ is small, in other materials ΔS_+ can influence substantially the resulting BC effects and therefore this contribution cannot be left out. For instance, ΔS_+ accounts for a large decrease of the BC effects in ammonium sulphate[30] whereas, more interestingly, it has been demonstrated that neglecting ΔS_+ in the plastic crystal Neopentylglycol ($[(CH_3)_2C(CH_2OH)_2]$, NPG) as done elsewhere[6] would omit a 25% increase in ΔS at 5 kbar[5]. In the compounds analyzed here, ΔS_+ becomes particularly significant for NPA, as shown in Fig. 3(a,b).

On the other hand, it is worth noticing here that ΔS_+ included in phase II, together with the knowledge of the transition entropy change $\Delta S_{\mathrm{II}\leftrightarrow\mathrm{I}}$ (shown in Figs 2i-l) and C_p, determines univocally ΔS_+ in phase I. Therefore, the experimental determination of ΔS_+ in phase I can be used to ascertain the consistency and uncertainty of different types of measurements. All the compounds studied here show[40] $(\partial V/\partial T)_{p_{\mathrm{atm}}}(\mathrm{I}) \geq (\partial V/\partial T)_{p_{\mathrm{atm}}}(\mathrm{II})$, from which we can deduce that $\Delta S_+(\mathrm{I}) \geq \Delta S_+(\mathrm{II})$. This inequality, along with the fact that in both phases the entropy varies with temperature similarly, mathematically imposes $\Delta S_{\mathrm{II}\leftrightarrow\mathrm{I}}$ to be roughly constant or to decrease when increasing pressure. Indeed, this is consistent with pressure-dependent transition entropy change for the endothermic ($\Delta S_{\mathrm{II}\to\mathrm{I}}$) and exothermic ($\Delta S_{\mathrm{I}\to\mathrm{II}}$) transitions (see Fig. 2i-l) derived from integration of $(1/T)dQ/|dT|$. In particular, we find that $\Delta S_{\mathrm{II}\leftrightarrow\mathrm{I}}$ for PG and AMP, and $\Delta S_{\mathrm{II}\to\mathrm{I}}$ for TRIS are roughly independent of pressure, but for TRIS $\Delta S_{\mathrm{I}\to\mathrm{II}}$ decreases according to $d\Delta S_{\mathrm{I}\to\mathrm{II}}/dp = -19 \pm 6$ J K^{-1} kg^{-1} kbar^{-1} whereas for NPA $d\Delta S_{\mathrm{II}\to\mathrm{I}}/dp = -4 \pm 2$ J K^{-1} kg^{-1} kbar^{-1} and $d\Delta S_{\mathrm{I}\to\mathrm{II}}/dp = -10 \pm 2$ J K^{-1} kg^{-1} kbar^{-1}.

4.4 Barocaloric response

By subtracting isobaric entropies at different pressures following adiabatic and isothermal paths, we have obtained the irreversible isothermal entropy changes $\Delta S(p_1 \to p_2) = S(T,p_2) - S(T,p_1) = S'(T,p_2) - S'(T,p_1)$ and adiabatic temperature changes $\Delta T(p_1 \to p_2) = T(S,p_2) - T(S,p_1) = T(S',p_2) - T(S',p_1)$ where the lower pressure will be taken always as atmospheric pressure p_{atm}. In materials displaying conventional BC effects, $dT_{\mathrm{II}\leftrightarrow\mathrm{I}}/dp > 0$ entails that compression-induced transitions are exothermic whereas decompression-induced transitions are endothermic. Therefore, BC effects on compression are computed from cooling runs and BC effects on decompression from heating runs (see Fig. 4). Irreversible ΔS achieves colossal values in all cases at small pressures, reaching on average over compression and decompression up to 600 ± 60 J K^{-1} kg^{-1} and 8 ± 2 K under 2.5 kbar for TRIS, 510 ± 50 J K^{-1} kg^{-1} and 22 ± 2 K under 2.5 kbar for PG, 690 ± 70 J K^{-1} kg^{-1} and 15.5 ± 2.0 K under 2.5 kbar for AMP and 330 ± 30 J K^{-1} kg^{-1} and 35 ± 5 K under 2.7 kbar for NPA, that increase up to 500 ± 50 J K^{-1} kg^{-1} and 62 ± 6 K under 5.9 kbar. Although these values are impressive, they are unuseful to determine the adequacy of a material for implementation in a real device because they cannot be reproduced cyclically after the first pressure change.

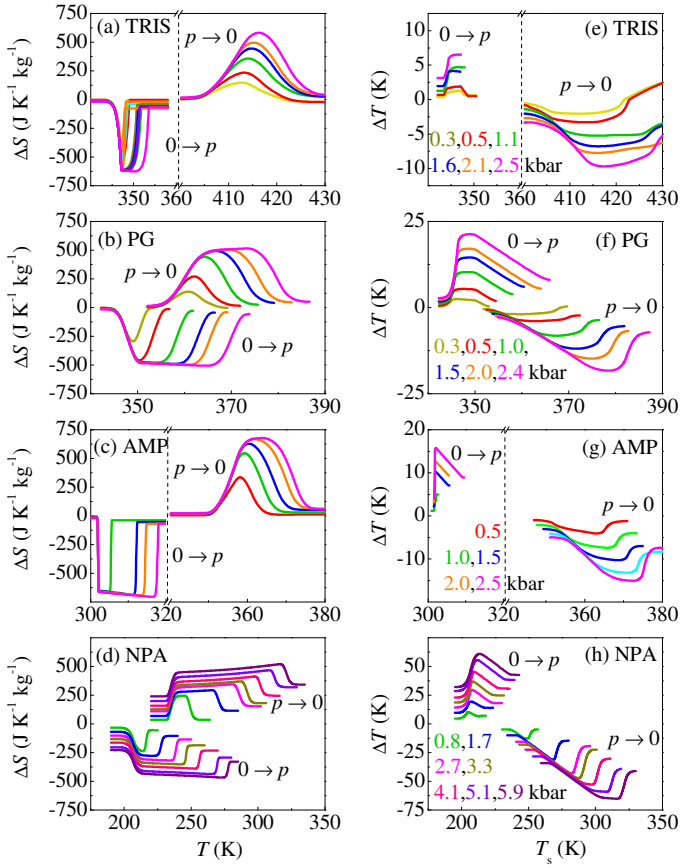

Fig. 4 (a-d) Isothermal entropy changes as a function of temperature and (e-h) adiabatic temperature changes as a function of the starting temperature T_s, under application and removal of selected pressures in (a,e) TRIS, (b,f) PG, (c,g) AMP and (d,h) NPA.

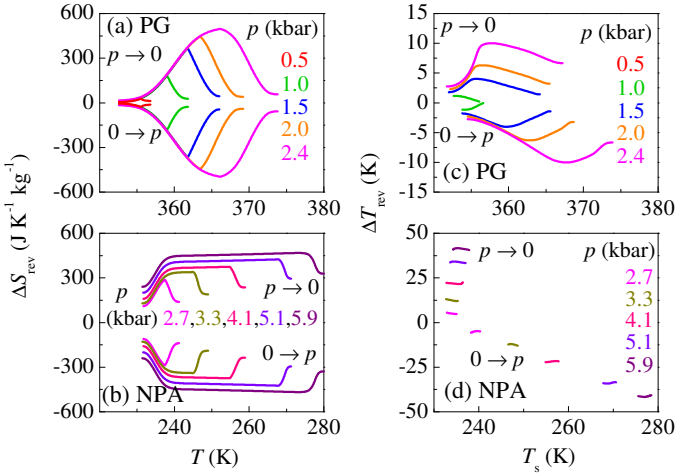

Fig. 5 (a,b) Reversible isothermal entropy changes as a function of temperature and (c,d) reversible adiabatic temperature changes as a function of the starting temperature T_s, under application and removal selected pressures in (a,c) PG and (b,d) NPA. For NPA, ΔT_{rev} is shown only within the temperature interval where the adiabatic path starts and finishes at the transition.

As discussed previously, reversible entropy changes, ΔS_{rev}, are computed quasi-directly as the overlapping between ΔS obtained on compression and decompression[11] whereas reversible adiabatic temperature changes, ΔT_{rev} are determined from adiabatic differences between $T(S, p_{atm})$ on heating and $T(S, p)$ on cooling[52]. The corresponding results confirm the aforementioned conclusions: BC effects in AMP and TRIS are irreversible within the whole pressure range analyzed here. Instead, for PG reversible effects (see 5a,c) are found above $p_{rev} \sim 0.4$ kbar, displaying $\Delta S_{rev} = 490 \pm 50$ J K^{-1} kg^{-1} and $\Delta T_{rev} = 10 \pm 1$ K under $p \sim 2.4$ kbar. In turn, reversible effects (see Fig. 5b,d) are found above $p_{rev} \sim 1.9$ kbar in NPA, displaying $\Delta S_{rev} = 290 \pm 30$ J K^{-1} kg^{-1} and $\Delta T_{rev} = 16 \pm 2$ K under $p \sim 2.6$ kbar, and $\Delta S_{rev} = 470 \pm 50$ J K^{-1} kg^{-1} and $\Delta T_{rev} = 42 \pm 4$ K under $p \sim 5.8$ kbar.

Figure 6 shows a summary of the maximum absolute irreversible (panels a-c) and reversible (d-f) BC effects as a function of the applied pressure for the compounds under study. Data for NPG[5] belonging to the same plastic crystal family, are also displayed for comparison.

The reversible values obtained for NPA and PG are comparable to the thermal response of harmful fluids used in current refrigerators[61] yet generated by greenhouse emission-free materials. Therefore, they are excellent candidates to be employed in future more sustainable cooling devices. The low thermal conductivity of our compounds can be palliated by an appropriate design that maximizes the surface-to-volume ratio such as powdered material embedded into graphite matrices[62] or the introduction of high thermal conductive nanoparticles[63]. It must be noted here that, in terms of safety, NPA is classified[64] as a flammable solid (flash point of 301 K), which should be taken into account for applications at room temperature. Instead, for PG[65] (and AMP[66] and TRIS[67]) no relevant hazards are identified.

5 Conclusions

We have studied the barocaloric response of four plastic crystals derived from neopentane across their ordered-orientationally disordered solid-state phase transition. For this purpose we have constructed isobaric entropy-temperature curves below, across and above the transition using our high-pressure calorimetry, and temperature-dependent heat capacity and volume from literature. The latter accounts for additional entropy changes due to thermal expansion of each phase, which appears to be important for NPA and negligible within error for the remaining compounds.

We have shown that to provide useful information for technological applications, the characterization of the reversible BC effects from high-pressure properties must be carried out. As a result, while all compounds studied here show outstanding BC properties upon the first application or removal of pressure, those plastic crystals having a bcc structure (AMP and TRIS) display too large hysteresis to be overcome by application of reasonable pressures and therefore they can be discarded as promising BC materials. Instead, those plastic crystals with an fcc structure (PG and NPA) transform more easily to the ordered phase, and therefore do show colossal reversible effects at moderate pressures. Our study reinforces the recently demonstrated great reversible BC potential of some plastic crystals for future cooling devices and should incite future works on caloric compounds to

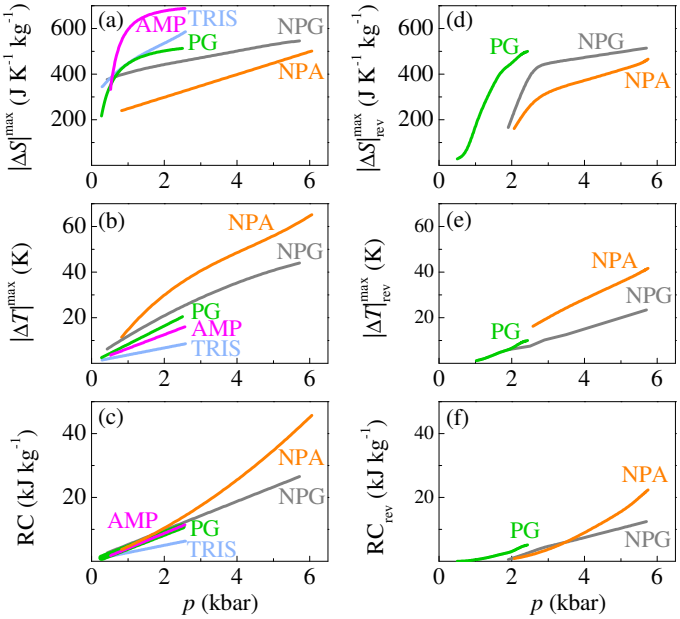

Fig. 6 (a) Maximum isothermal entropy changes, (b) maximum adiabatic temperature changes, and (c) refrigerant capacity as a function of pressure, fitted on joint data under first removal and application of pressure. (d) Maximum isothermal entropy changes, (e) maximum adiabatic temperature changes, and (f) refrigerant capacity as a function of pressure for reversible cycles. NPG stands for neopentylglycol and the corresponding data, calculated from Ref.[5], haven been included for completeness and comparison.

systematically provide reversible values as a way to accelerate the development of advanced materials for environmentally-friendly solid-state refrigeration.

Conflicts of interest

The use of the compounds studied in this work and other plastic crystals for barocaloric cooling is covered in the following patent: X. Moya, A. Avramenko, L. Mañosa, J.-Ll. Tamarit and P. Lloveras, Use of barocaloric materials and barocaloric devices, PCT/EP2017/076203 (2017). The remaining authors declare no conflicts of interests.

Acknowledgements

This work was supported by the MINECO projects MAT2016-75823-R and FIS2017-82625-P, the DGU project 2017SGR-42, the UK EPSRC grant EP/M003752/1, and the ERC Starting grant no. 680032. X. M. is grateful for support from the Royal Society.

Notes and references

1 *Energy Savings Potential and RD&D Opportunities for Non-Vapor-Compression HVAC Technologies*, `https://www.energy.gov/sites/prod/files/2014/03/f12/Non-Vapor%20Compression%20HVAC%20Report.pdf`, (accessed July 2019).

2 X. Moya, S. Kar-Narayan and N. D. Mathur, *Nat. Mater*, 2014, **13**, 439 – 450.

3 L. Mañosa and A. Planes, *Adv. Mater.*, 2017, **29**, 1603607.

4 A. Kitanovski, U. Plaznik, U. Tomc and A. Poredos, *Int. J. Refrig.*, 2015, **57**, 288 – 298.

5 P. Lloveras, A. Aznar, M. Barrio, P. Negrier, C. Popescu, A. Planes, L. Mañosa, E. Stern-Taulats, A. Avramenko, N. D. Mathur, X. Moya and J.-L. Tamarit, *Nat. Commun.*, 2019, **10**, 1803.

6 B. Li, Y. Kawakita, S. Ohira-Kawamura, T. Sugahara, H. Wang, J. Wang, Y. Chen, S. I. Kawaguchi, S. Kawaguchi, K. Ohara, K. Li, D. Yu, R. Mole, T. Hattori, T. Kikuchi, S.-I. Yano, Z. Zhang, Z. Zhang, W. Ren, S. Lin, O. Sakata, K. Nakajima and Z. Zhang, *Nature*, 2019, **567**, 506–510.

7 D. K. Benson, W. Burrows and J. D. Webb, *Sol. Energy Mat.*, 1986, **13**, 133–152.

8 M. Barrio, J. Font, D. O. López, J. Muntasell and J.-L. Tamarit, *Sol. Energy Mater. Sol. Cells*, 1992, **27**, 127 – 133.

9 P. J. Shamberger and F. S. Ohuchi, *Phys. Rev. B*, 2009, **79**, 144407.

10 T. Krenke, S. Aksoy, E. Duman, M. Acet, X. Moya, L. Mañosa and A. Planes, *J. Appl. Phys.*, 2010, **108**, 043914.

11 B. Emre, S. Yüce, E. Stern-Taulats, A. Planes, S. Fabbrici, F. Albertini and L. Mañosa, *J. Appl. Phys.*, 2013, **113**, 213905.

12 D. Matsunami, A. Fujita, K. Takenaka and M. Kano, *Nat. Mater.*, 2014, **14**, 73 – 78.

13 R. R. Wu, L. F. Bao, F. X. Hu, Q. Z. Huang, J. Wang, X. L. Dong, G. N. Li, J. R. Sun, F. R. Shen, T. Y. Zhao, X. Q. Zheng, L. C. Wang, Y. Liu, W. L. Zuo, Y. Y. Zhao, M. Zhang, Z. C. Wang, C. Q. Jin, G. H. Ro, X. F. Han and B. G. Shen, *Sci. Rep.*, 2015, **5**, 18027.

14 T. Samanta, P. Lloveras, A. U. Saleheen, D. Lepkowski, E. Kramer, I. Dubenko, P. Adams, D. Young, M. Barrio, J.-L. Tamarit, N. Ali and S. Stadler, *Appl. Phys. Lett.*, 2018, **112**, 021907.

15 S. Lin, O. Tegus, E. Brück, W. Dagula, T. J. Gortnemulder and K. H. J. Buschow, *IEEE Trans Magn*, 2006, **42**, 3776–78.

16 L. Caron, N. T. Trung and E. Brück, *Phys. Rev. B*, 2011, **84**, 020414(R).

17 Q. Ren, W. Hutchison, J. Wang, A. Studer and S. Campbell, *J. Alloys Compds*, 2017, **693**, 32–39.

18 M. Barrio, J. Font, D. O. López, J. Muntasell and J.-L. Tamarit, *J. Therm. Anal.*, 1994, **41**, 1771–1775.

19 J.-L. Tamarit, B. Legendre and J. M. Buisine, *Mol. Cryst. Liq. Cryst.*, 1994, **250**, 347 – 358.

20 J. Salud, D. O. López, M. Barrio and J. L. Tamarit, *J. Mater. Chem.*, 1999, **9**, 909–916.

21 L. Caron, Z. Ou, T. Nguyen, D. C. Thanh, O. Tegus and E. Brück, *J. Magn. Magn. Mat.*, 2009, **321**, 3559 – 3566.

22 R. Niemann, O. Heczko, L. Schultz and S. Fähler, *Int. J. Refrig.*, 2014, **37**, 281–288.

23 J. S. Young, *PhD thesis*, University of Cambridge, 2012.

24 Y. Liu, J. F. Scott and B. Dkhil, *Appl. Phys. Rev.*, 2016, **3**, 031102.

25 J. Li, J. Li, S. Qin, X. Su, L. Qiao, Y. Wang, T. Lookman and Y. Bai, *Phys. Rev. Appl.*, 2019, **11**, 044032.

26 T. Gottschall, E. Stern-Taulats, L. Mañosa, A. Planes, K. P.

Skokov and O. Gutfleisch, *Appl. Phys. Lett.*, 2017, **110**, 223904.
27 P. W. Bridgman, *Proc. Am. Acad. Arts Sci.*, 1915, **51**, 55 – 124.
28 A. Aznar, P. Lloveras, J. Kim, M. Barrio, J.-L. Tamarit, C.-F. Sánchez-Valdés, J.-L. Sánchez-Llamazares, N. D. Mathur and X. Moya, *Adv. Mater.*, 2019, **31**, 1903577.
29 P. Lloveras, T. Samanta, M. Barrio, I. Dubenko, N. Ali, J.-L. Tamarit and S. Stadler, *APL Materials*, 2019, **7**, 061106.
30 P. Lloveras, E. Stern-Taulats, M. Barrio, J.-L. Tamarit, S. Crossley, W. Li, V. Pomjakushin, A. Planes, L. Mañosa, N. D. Mathur and X. Moya, *Nat. Commun.*, 2015, **6**, 8801.
31 E. Stern-Taulats, P. Lloveras, M. Barrio, E. Defay, M. Egilmez, A. Planes, J.-L. Tamarit, L. Mañosa, N. D. Mathur and X. Moya, *APL Mater.*, 2016, **4**, 091102.
32 J. M. Bermúdez-García, M. Sánchez-Andújar, S. Castro-García, J. López-Beceiro, R. Artiaga and M. A. Senarís-Rodríguez, *Nat. Commun.*, 2017, **8**, 15715.
33 Z. Y. Zhang and M. L. Yang, *Thermochim. Acta*, 1990, **169**, 263–269.
34 A. Saxena and T. Lookman, in *Ferroic Domain Structures using Ginzburg-Landau Methods*, ed. S. Yip, Springer Netherlands, Dordrecht, 2005, pp. 2143–2155.
35 N. P. Kobelev, R. K. Nikolaev, N. S. Sidorov and Y. M. Soifer, *Phys. Solid State*, 2001, **43**, 2344–2350.
36 J. L. Schlenker, G. V. Gibbs and M. B. Boisen Jr, *Acta Cryst.*, 1978, **A34**, 52–54.
37 R. Sandrock and G. Scheneider, *Ber. Bunsenges. Phys. Chem.*, 1983, **87**, 197–201.
38 M. Jenau, J. Reuter, J.-L. Tamarit and A. Würflinger, *J. Chem. Soc. Faraday Trans.*, 1996, **92**, 1899 – 1904.
39 J. Salud, M. Barrio, D. O. López, J.-L. Tamarit and X. Alcobé, *J. Appl. Cryst.*, 1998, **31**, 748–757.
40 A. Aznar, P. Lloveras, M. Barrio and J.-L. Tamarit, *Eur. Phys. J. Spec. Top.*, 2017, **226**, 1017–1029.
41 J. Font, J. Muntasell and E. Cesari, *Mater. Res. Bull.*, 1995, **30**, 839 – 844.
42 D. Eilerman and R. Rudman, *J. Chem. Phys.*, 1980, **72**, 5656 – 5666.
43 M. Zuriaga, L. C. Pardo, P. Lunkenheimer, J. L. Tamarit, N. Veglio, M. Barrio, F. J. Bermejo and A. Loidl, *Phys. Rev. Lett.*, 2009, **103**, 075701.
44 M. Romanini, P. Negrier, J.-L. Tamarit, S. Capaccioli, M. Barrio, L. C. Pardo and D. Mondieig, *Phys. Rev. B*, 2012, **85**, 134201.
45 P. Negrier, M. Barrio, J. L. Tamarit, L. C. Pardo and D. Mondieig, *Cryst. Growth Des.*, 2012, **12**, 1513–1519.
46 P. Negrier, J. L. Tamarit, M. Barrio and D. Mondieig, *Cryst. Growth Des.*, 2013, **13**, 782–791.
47 B. B. Hassine, P. Negrier, M. Romanini, M. Barrio, R. Macovez, A. Kallel, D. Mondieig and J. L. Tamarit, *Phys. Chem. Chem. Phys.*, 2016, **18**, 10924.
48 E. D. Emmons, J. C. Fallas, V. K. Kamisetty, W.-M. Chien, A. M. Covington, R. S. Chellappa, S. A. Gramsch, R. J. Hemley and D. Chandra, *J. Phys. Chem. B*, 2010, **114**, 5649–5656.
49 B. B. Hassine, P. Negrier, M. Barrio, D. Mondieig, S. Massip and J. L. Tamarit, *Cryst. Growth Des.*, 2015, **15**, 4149–4155.
50 G. B. Guthrie and J. P. McCullough, *J. Phys. Chem. Solids*, 1961, **18**, 53 – 61.
51 B. Granzow, *J. Mol. Struct.*, 1996, **381**, 127–131.
52 E. Stern-Taulats, A. Gràcia-Condal, A. Planes, P. Lloveras, M. Barrio, J.-L. Tamarit, S. Pramanick, S. Majumdar and L. Mañosa, *Appl. Phys. Lett.*, 2015, **107**, 152409.
53 A. Aznar, P. Lloveras, M. Romanini, M. Barrio, J.-L. Tamarit, C. Cazorla, D. Errandonea, N. D. Mathur, A. Planes, X. Moya and L. Mañosa, *Nat. Commun.*, 2017, **8**, 1851.
54 M. Straka, A. van Genderen, K. Ruzicka and V. Ruzicka, *J. Chem. Eng. Data*, 2007, **52**, 794 – 802.
55 T. Bo, T. Zhi-Cheng, L. Rui-Bin, M. Chang-Gong and Z. Jing-Nan, *Energy Convers. Manag.*, 2010, **51**, 1905–1910.
56 D. Chandra, W.-M. Chien, V. Gandikotta and D. W. Lindle, *Z. Phys. Chem.*, 2002, **216**, 1433–1444.
57 K. Arvidsson and E. F. Westrum Jr., *J. Chem. Thermodyn.*, 1972, **4**, 449–453.
58 S. Divi, R. Chellappa and D. Chandra, *J. Chem. Thermodyn.*, 2006, **38**, 1312–1326.
59 W.-M. Chien, I. Gantan, A. Mishra, D. Chandra, V. Kamisetty and P. Mekala, in *Phase Equilibrium and Characterization Studies of Binary Organic Thermal Energy Storage Materials*, ed. S. Wang, J. E. Dutrizac, M. L. Free, J. Y. Hwang and D. Kim, John Wiley & Sons, Hoboken, USA, 2012, pp. 461–470.
60 M. Barrio, *PhD thesis*, University of Barcelona, 1993.
61 M. O. McLinden, *Thermophysical properties of refrigerants. ASHRAE Handbook: Fundamentals*, ASHRAE, Atlanta, 2009.
62 X. Wang, Q. Guo, Y. Zhong, X. Wei and L. Liu, *Renew. Energ.*, 2013, **51**, 241 – 246.
63 K. Solangi, S. Kazi, M. Luhur, A. Badarudin, A. Amiri, R. Sadri, M. Zubir, S. Gharehkhani and K. Teng, *Energy*, 2015, **89**, 1065 – 1086.
64 https://www.sigmaaldrich.com/catalog/product/aldrich/n7206?lang=en&region=GB, (accessed October 2019).
65 https://www.sigmaaldrich.com/catalog/product/aldrich/t87807?lang=en&region=GB, (accessed October 2019).
66 https://www.sigmaaldrich.com/catalog/product/sigma/a9754?lang=en&region=GB, (accessed October 2019).
67 https://www.sigmaaldrich.com/catalog/product/sigma/t1503?lang=en&region=GB, (accessed October 2019).